https://doi.org/10.1016/j.ymssp.2020.107232

This is the Pre-Published Version.

# Prediction Model for Sound Radiation from an Unbaffled Long Enclosure with the Ground Effect

Weiping Yang, Zhibo Wang, Yatsze Choy*

Department of Mechanical Engineering, The Hong Kong Polytechnic University, Hung Hom, Kowloon, Hong Kong SAR, People's Republic of China

* Corresponding author.
E-mail address: mmyschoy@polyu.edu.hk (Y. S. Choy).



© 2020. This manuscript version is made available under the CC-BY-NC-ND 4.0 license http://creativecommons.org/licenses/by-nc-nd/4.0/

# A B S T R A C T

A theoretical model is presented for the prediction of sound radiation from a semi-infinite unbaffled long enclosure with the ground effect. This geometrical arrangement forms an idealized representation of traffic facilities such as tunnels and railway stations where noise propagates along the long enclosures and radiates to the outside through the openings. Despite the fact that the model described here applies only to idealized situations, it contains essential elements of realistic configurations, which is conducive to understanding the physics of the sound radiation phenomenon and significant for the proposal of appropriate noise control strategies. First of all, by expressing the sound field in terms of the superposition of propagating modes inside the long enclosure and adopting the Fourier transform technique in other regions, the unsolvable boundary value problem in the natural domain is reduced to a scalar modified Wiener-Hopf (W-H) equation of the second kind in the spectral domain. Then, its solution is obtained using the standard factorization and decomposition procedures, and the radiated sound field is attained through the inverse Fourier transform technique, which involves a contour integral that can be evaluated approximately via the saddle point method. After that, the model is validated by the finite element method (FEM), and the far-field directivity patterns of the radiated sound fields are presented. Finally, the properties of the sound fields both inside and outside three enclosures with different boundary conditions are analyzed, based on which potential noise reduction methods by using acoustic liners are discussed.



**Keywords:** Sound radiation, Unbaffled long enclosure, Wiener-Hopf technique.

# 1. Introduction

Long enclosures [1, 2], with lengths that are much greater than their widths and heights, can be commonly observed in traffic facilities such as tunnels, railway and underground stations. Such enclosures provide people with great convenience but also cause a lot of acoustical problems. It is quite difficult for the sound energy inside a long enclosure to dissipate, which will result in a high sound pressure level (SPL) and a long reverberation time. Such an acoustical environment will produce negative impacts on drivers and passengers and simultaneously impair speech intelligibility. In addition, as noise cannot be transmitted to the outside directly through the wall, it will concentrate at both ends of the enclosure and radiate to the outside through the openings. Taking tunnel for instance, if there are residents near the portals, their living and working conditions will be severely deteriorated [3]. Thus, it is of great significance to understand the formation mechanisms of sound fields both inside and outside a long enclosure so that suitable methods can be applied to control them.

Due to the geometrical similarity between a long enclosure and a duct, sound field inside a long enclosure can be predicted by the classical wave theory and the image source method (ISM), which are frequently used in the duct acoustics [4, 5]. Whereas, a disadvantage of the usual energy-based ISM is that it excludes the interferences between multiple reflections and the phase information of each image. To optimize the model, a coherent ISM [6, 7] was proposed and developed, which can take the phase change of each reflection on the boundary into consideration. Nevertheless, all the models mentioned above can only be applied to calculate the sound field inside an infinite long enclosure because they cannot include the reflected sound wave produced by the radiation impedance at the opening.

Sound radiation from a long enclosure has been an important subject both in the diffraction theory and the mathematics. The characteristics of a radiated sound field depend not only on the properties of the acoustic source but also on the geometry of the long enclosure and the way it is terminated, which is normally

either baffled or unbaffled. For sound radiation from a baffled long enclosure, the Rayleigh integral can be applied [8], which is reasonably straightforward and thoroughly introduced in the book written by Pierce [9]. However, this method cannot predict the sound field at the backside of the enclosure, which limits its application in practice. For sound radiation from an unbaffled long enclosure, Levine and Schwinger [9] proposed a rigorous model to predict the radiation of plane wave from an unflanged pipe based on the Wiener-Hopf (W-H) technique. Subsequently, the model was extended to include the radiation of higher-order modes [11]. The directivity pattern of the radiated sound field was analyzed, and practical strategies were proposed to predict the lobes, zeros and sidelines [12]. These solutions, however, are not convenient for numerical calculations because they are generally expressed in terms of complex integrals. To simplify the problem, several approximation methods were also proposed, among which the most widely used one is Hocter's method [13, 14]. It is based on the ray structures of duct modes propagating inside a semi-infinite cylindrical duct [15]. Then, in conjunction with Keller's geometrical theory of diffraction (GTD) [16], the radiation patterns of modes can be easily expressed. However, the model is mainly applicable to cylindrical ducts, and the radiated field is assumed to be free. Besides, only plane-wave and single-mode incidences were considered in the models mentioned above. Consequently, these models are commonly applied in the prediction of noise radiated from heating, ventilation and air-conditioning (HVAC) systems, exhaust stacks in industrial power plants and turbofan aero engines.

Apart from analytical models, numerical methods were also proposed to calculate the sound level radiated from long enclosures. By introducing a perfectly matched layer (PML) outside an enclosure, the unbounded radiation problem was converted into a waveguide problem that can be solved by the finite element method (FEM) [17]. However, to obtain an accurate solution, the PML parameters need to be optimized during numerical calculations, which rely greatly on personal experience. To avoid the use of PML, a hybrid method was developed [18] to couple the inside and outside regions, where the inside

region was treated by a normal mode expansion and the outside region was discretized by finite elements. Such hybrid methods perform well in general configurations. For a large-size model, however, the calculation efficiency declines rapidly due to the sharp growth in the number of elements, limiting the application of these models to real traffic facilities.

A large difference between the problem at hand and the existing radiation models is that, the ground effect is taken into account. As a result, the acoustic domain outside the enclosure becomes a semi-infinite region rather than a free region. For such a geometrical configuration, it is difficult to obtain an analytical solution to the sound radiation problem, and the aforementioned prediction models cannot be applied directly. For engineering applications, the Research Committee on Road Traffic Noise of the Acoustical Society of Japan published the ASJ model [19] to predict the noise radiated from traffic tunnels in which correction terms for the diffraction at the sharp edge and the ground effect were included. However, these terms were either from the experimental data published by Maekawa [20] or empirical coefficients, which will lead to a low accuracy. Moreover, the ASJ model is an energy-based method, and the results do not contain the phase information. Enlightened by the ASJ model, Heutschi and Bayer [3] proposed a similar model for the prediction of tunnel noise in which the radiated sound field was expressed in terms of the directivity pattern and the damping effects. However, the details on how to obtain these expressions were not mentioned. For this kind of radiation problem, in brief, research is still in the exploration stage.

The W-H technique has been frequently used in solving certain kinds of radiation problems. It was initially proposed to solve electromagnetic problems regarding wave radiation from an impedance-loaded parallel plate waveguide and a horn radiator [21, 22]. Several years later, the technique was extended to tackle acoustical problems [23-26]. Sound radiation from an unbaffled annular jet pipe was formulated by the technique [23]. Then, the model was further developed to include lined boundary conditions [24]. These models are important for acoustical aircraft-engine engineering applications and for understanding the

physics behind the sound radiation phenomenon. Additionally, the transmission loss (TL) of a cylindrical duct with an acoustically lined muffler [25] and a circular silencer with a locally reacting lining [26] were analyzed based on this method. From these research findings, certain types of linear partial differential equations subjected to impedance boundary conditions on semi-infinite geometries can be solved by using the W-H technique. Accordingly, for sound radiation from a long enclosure with the ground effect and impedance conditions, the method will also be applicable.

Instead of predicting and analyzing the sound fields inside and outside a long enclosure separately, as in most of the literature, we try to establish an analytical model based on the W-H technique that can predict the interior and the exterior sound fields simultaneously. Another important aspect addressed in this paper but not addressed in previous studies is the use of a monopole point source rather than a plane-wave or single-mode incidence to simulate the sound excitation. In summary, the objectives of this study are: 1). to propose a theoretical model for the prediction of the sound fields both inside and outside an unbaffled long enclosure in which the ground effect, semi-infinite boundary conditions and a monopole point source are taken into consideration; 2). to validate the correctness and accuracy of the proposed model through the FEM and examine its calculation efficiency for a large-size geometry; 3). to thoroughly analyze the properties of the sound fields when imposing different boundary conditions, understand their formation mechanisms and accordingly introduce potential strategies for the mitigation of noise.

The remainder of this paper is organized as follows. In section 2, a theoretical model is established to predict the sound fields both inside and outside an unbaffled long enclosure with the ground effect based on the W-H technique. In section 3, the model is validated, detailed discussions are presented, and based on which potential noise control strategies are introduced. Conclusions are drawn in section 4.

# 2. Theoretical modeling

## 2.1 Description of the problem in the natural domain

Consider the radiation of sound that is produced by a monopole point source of harmonic time dependence from a two-dimensional semi-infinite long enclosure with the ground effect. The height of the long enclosure is $L_y$, and the thickness of the wall is assumed to be zero for simplicity. The long enclosure extends to minus infinity, and the ground extends to plus infinity as shown in Fig. 1. The ground and the wall surfaces are characterized by acoustic impedances $Z_z$, where z=1, 2, 3, 4. The origin of the coordinate system is located at the intersection of the opening and the ground. The source is placed at $(x_0, y_0)$ near the ground. Imaginary interfaces I and II are depicted for the convenience of analysis. They divide the whole acoustic domain into three sub-regions A, B and C, which will be analyzed separately later.

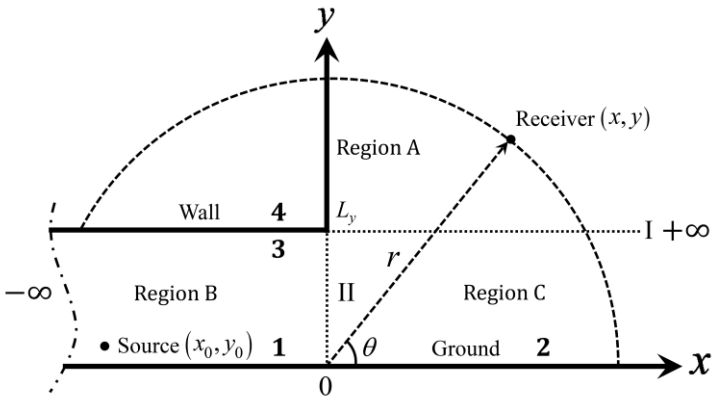


Fig. 1. Schematic diagram of sound radiation from an unbaffled long enclosure with the ground effect.

According to the partition of the acoustic domain in Fig. 1, it is convenient to express the total sound pressure field by the following piecewise function as

$$p_{total}(x,y)=\begin{cases} p_A(x,y) & x\in(-\infty,+\infty)\cap y\in\left[L_y,+\infty\right) \\ p_B^{inc}(x,y)+p_B(x,y) & x\in(-\infty,0]\cap y\in\left[0,L_y\right], \\ p_C(x,y) & x\in[0,+\infty)\cap y\in\left[0,L_y\right] \end{cases} \tag{1}$$

where $p_B^{inc}(x,y)$ and $p_B(x,y)$ are the incident and reflected sound pressure fields of region B, respectively. $p_A(x,y)$ and $p_C(x,y)$ are the scattered sound pressure fields of regions A and C, respectively. The total sound pressure field satisfies the homogeneous Helmholtz equation:

$$\left(\frac{\partial^2}{\partial x^2}+\frac{\partial^2}{\partial y^2}+k^2\right)p_{total}(x,y)=0, \tag{2}$$

where $k$ represents the wavenumber in free space. Notably, in any physical medium, loss is inevitable. Therefore, an ideal lossless medium, which is often used in theoretical analysis, can be regarded as a limiting case with a vanishingly small loss. For mathematical convenience, we assume that

$$k=k_1-ik_2, \quad k_1 \gg k_2 > 0, \tag{3}$$

where $k_1$ and $-k_2$ denote the real and imaginary parts of $k$, respectively. The boundary condition at each surface can be expressed as

$$\frac{\partial p_B(x,0)}{\partial y}-\frac{i\rho k c_0 p_B(x,0)}{Z_1}=0, \quad x\in(-\infty,0], \tag{4}$$

$$\frac{\partial p_C(x,0)}{\partial y}-\frac{i\rho k c_0 p_C(x,0)}{Z_2}=0, \quad x\in[0,+\infty), \tag{5}$$

$$\frac{\partial p_B(x,L_y)}{\partial y}+\frac{i\rho k c_0 p_B(x,L_y)}{Z_3}=0, \quad x\in(-\infty,0], \tag{6}$$

$$\frac{\partial p_A(x,L_y)}{\partial y}-\frac{i\rho k c_0 p_A(x,L_y)}{Z_4}=0, \quad x\in(-\infty,0], \tag{7}$$

where $c_0$ is the speed of sound, and $\rho$ is the density of air. At the imaginary interfaces I and II, the continuity relations of the sound pressure and the normal particle velocity should be satisfied as

$$p_A(x,L_y)=p_C(x,L_y), \quad x\in[0,+\infty), \tag{8}$$

$$\frac{\partial p_A\left(x, L_y\right)}{\partial y} = \frac{\partial p_C\left(x, L_y\right)}{\partial y}, \quad x \in \left[0, +\infty\right), \tag{9}$$

$$p_B^{inc}\left(0, y\right) + p_B\left(0, y\right) = p_C\left(0, y\right), \qquad y \in \left[0, L_y\right], \tag{10}$$

$$\frac{\partial p_B^{inc}\left(0, y\right)}{\partial x} + \frac{\partial p_B\left(0, y\right)}{\partial x} = \frac{\partial p_C\left(0, y\right)}{\partial x}, \qquad y \in \left[0, L_y\right]. \tag{11}$$

When boundaries at infinity and geometrical singularities are involved, several mathematically acceptable solutions of the acoustic field of interest might be obtained. However, only one of them is completely consistent with the anticipated physical phenomenon. Therefore, in order to ensure the uniqueness of the solution to the problem at hand, we have to consider the Sommerfeld radiation condition [27] at infinity

$$\lim_{r \to \infty} \sqrt{r}\left[\frac{\partial p_{total}\left(r, \theta\right)}{\partial r} - ikp_{total}\left(r, \theta\right)\right] = 0, \quad r = \sqrt{x^2 + y^2}\,, \tag{12}$$

and the edge condition, which requires that the acoustical energy stored in any finite neighborhood of the sharp edge should be finite [28], namely,

$$p_{total}\left(x, L_y\right) = O\left(\left|x\right|^{1/2}\right), \quad \frac{\partial p_{total}\left(x, L_y\right)}{\partial y} = O\left(\left|x\right|^{-1/2}\right), \ \left|x\right| \to 0\,. \tag{13}$$

The definitions of distance $r$ and observation angle $\theta$ can be seen in Fig. 1. The incident sound pressure field of region B, which is produced by a monopole point source of harmonic time dependence, satisfies the following inhomogeneous partial differential equation [4]:

$$\nabla^2\left[p_B^{inc}\left(x, y\right)e^{i\omega t}\right] - \frac{1}{c_0^2}\frac{\partial^2}{\partial t^2}\left[p_B^{inc}\left(x, y\right)e^{i\omega t}\right] = -\rho\frac{\partial}{\partial t}\left(Q_0 e^{i\omega t}\right)\delta\left(x - x_0\right)\delta\left(y - y_0\right), \tag{14}$$

where $\nabla^2$ is the two-dimensional Laplace operator, $Q_0$ denotes the volume velocity strength and $\delta$ is the Dirac delta function. The time-dependent factor $e^{i\omega t}$, where $\omega$ is angular frequency and $t$ is time, is well known and will be suppressed throughout. Based on Eqs. (4) and (6), the solution of Eq. (14) can be obtained:

$$p_B^{inc}(x,y)=\frac{\rho k c_0 Q_0}{2}\sum_{n=0}^{N}\frac{Y_n^B(y_0)Y_n^B(y)}{N_n^B\phi_n}e^{-i\phi_n|x-x_0|}, \tag{15}$$

where $N$ is the maximum number of truncated mode series. The transversal modal function of region B is given by

$$Y_n^B(y)=\cos(\xi_n y)+\frac{i\rho k c_0\sin(\xi_n y)}{Z_1\xi_n}. \tag{16}$$

The transversal wavenumbers satisfy the following characteristic equation:

$$L(\xi_n)=i\rho k c_0\left(\frac{1}{Z_1}+\frac{1}{Z_3}\right)\cos(\xi_n L_y)-\left(\xi_n^2+\frac{k^2\rho^2c_0^2}{Z_1Z_3}\right)\frac{\sin(\xi_n L_y)}{\xi_n}=0. \tag{17}$$

The normalized coefficient of the transversal modal function can be obtained as

$$N_n^B=\lim_{\xi\to\xi_n}\int_0^{L_y}Y^B(y)Y_n^B(y)dy=Y_n^B(L_y)\frac{dL(\xi_n)}{2\xi_n}. \tag{18}$$

The propagating wavenumber along the horizontal direction is given by

$$\phi_n=\sqrt{k^2-\xi_n^2}. \tag{19}$$

Similarly, the reflected sound pressure field of region B can be expressed in terms of normal modes as

$$p_B(x,y)=\sum_{j=0}^{J}b_jY_j^B(y)e^{i\phi_j x}, \tag{20}$$

where $b_j$ denotes the modal response, and $J$ is the maximum number of truncated mode series. At this point, the boundary value problem is well defined in the natural domain. However, it is impossible to find a solution through conventional methods due to the complex geometry. Enlightened by the infinite limits in the Fourier integral, which can be applied to describe the semi-infinite acoustic domain outside a long enclosure, we aim to transform the problem into the spectral domain by using the Fourier transform technique and obtain the solution by the W-H technique, which is designed to solve problems with mixed and semi-infinite boundary conditions.

## 2.2 W-H equation in the spectral domain

The Helmholtz equation for region A can be converted into the complex $\alpha$-plane through the full-range Fourier transform in terms of $x$ as

$$\int_{-\infty}^{+\infty}\left[\frac{\partial^2 p_A(x,y)}{\partial x^2}+\frac{\partial^2 p_A(x,y)}{\partial y^2}+k^2 p_A(x,y)\right]e^{-i\alpha x}dx=0 \tag{21}$$

where $\alpha=\sigma+i\tau$ denotes the Fourier transform variable. The first term in the bracket of Eq. (21) can be integrated by parts as

$$\begin{aligned}&\int_{-\infty}^{+\infty}\frac{\partial^2 p_A(x,y)}{\partial x^2}e^{-i\alpha x}dx=\left[\frac{\partial p_A(x,y)}{\partial x}e^{-i\alpha x}\right]_{-\infty}^{+\infty}\\&+i\alpha\left[p_A(x,y)e^{-i\alpha x}\right]_{-\infty}^{+\infty}-\alpha^2\int_{-\infty}^{+\infty}p_A(x,y)e^{-i\alpha x}dx=-\alpha^2 P_A(\alpha,y)\end{aligned}, \tag{22}$$

where

$$P_A(\alpha,y)=\int_{-\infty}^{+\infty}p_A(x,y)e^{-i\alpha x}dx \tag{23}$$

is the transformed sound pressure field of region A in the complex $\alpha$-plane. The contributions from the bracketed terms of Eq. (22) at positive and negative infinity tend to be zero. This is due to the Sommerfeld radiation condition, which states that the outgoing wave disappears at infinity. The transformed Helmholtz equation for region A can be expressed as

$$\left[\frac{\partial^2}{\partial y^2}+K^2(\alpha)\right]P_A(\alpha,y)=0, \tag{24}$$

where $K(\alpha)=\sqrt{k^2-\alpha^2}$, which is called the square root function, is defined in the complex $\alpha$-plane with branch points $\pm k$ and branch cuts $C_{\pm}$ along $\alpha=k$ to $\alpha=k-i\infty$ and $\alpha=-k$ to $\alpha=-k+i\infty$ such that we have $K(0)=k$ as shown in Fig. 2. This is a compulsory choice due to the physical existence of the Green's function. Besides, it can be observed that the imaginary parts of the numbers in the cut plane are

all negative, which implies that, in this configuration, the cut plane is a proper sheet. For the convenience of the description later, we define that the region $\tau > -k_2$ is the upper half complex $\alpha$-plane and the region $\tau < k_2$ is the lower half complex $\alpha$-plane.

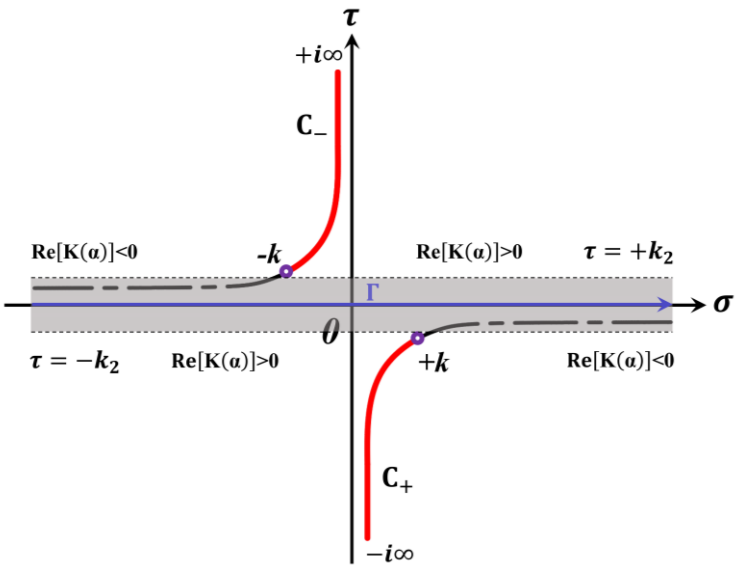


Fig. 2. Schematic diagram of branch points $\pm k$ (purple circles), branch cuts $C_{\pm}$ (red solid line) and the integration path $\Gamma$ for inverse Fourier transform (blue solid arrow line) in the complex $\alpha$-plane.

The transformed sound pressure field of region A in the complex $\alpha$-plane can be divided into two parts according to the definition of the half-range Fourier transform as

$$P_A(\alpha, y) = P_A^-(\alpha, y) + P_A^+(\alpha, y) = \int_{-\infty}^{0} p_A(x, y) e^{-i\alpha x} dx + \int_{0}^{+\infty} p_A(x, y) e^{-i\alpha x} dx \,. \tag{25}$$

Based on the following asymptotic behavior:

$$p_A(x, y) = O\left(e^{-ik|x|}\right), \quad x \to \pm\infty, \tag{26}$$

it can be easily observed that $P_A^+(\alpha, y)$ and $P_A^-(\alpha, y)$ are regular functions in the upper and lower half complex $\alpha$-planes, respectively. The general solution of Eq. (24) satisfying the Sommerfeld radiation condition can be expressed as

$$P_A(\alpha, y) = P_A^-(\alpha, y) + P_A^+(\alpha, y) = A(\alpha) e^{-iK(\alpha)(y-L_y)}, \tag{27}$$

where $A(\alpha)$ is an unknown spectral coefficient. Combining the transformed form of Eq. (7), Eq. (27) and its derivative with respect to *y*, the following identity can be obtained:

$$\left[\frac{\partial}{\partial y} - \frac{i\rho k c_0}{Z_4}\right] P_A^+(\alpha, L_y) = R^+(\alpha) = -i\left[K(\alpha) + \frac{\rho k c_0}{Z_4}\right] A(\alpha). \tag{28}$$

Here, $R^+(\alpha)$ is an important intermediate-term. Once this term is determined, the transformed sound pressure field of region A can be obtained. Using the inverse Fourier transform, the sound pressure field of region A in the natural domain can be attained.

On the other hand, the Helmholtz equation for region C can also be converted into the complex $\alpha$-plane by using the half-range Fourier transform with respect to $x$ as

$$\left[\frac{\partial^2}{\partial y^2} + K^2(\alpha)\right] P_C^+(\alpha, y) = f(y) + i\alpha g(y), \tag{29}$$

where the following definitions are used:

$$f(y) = \frac{\partial p_C(0, y)}{\partial x}, \quad g(y) = p_C(0, y) \tag{30}$$

and

$$P_C^+(\alpha, y) = \int_0^{+\infty} p_C(x, y) e^{-i\alpha x} dx \tag{31}$$

The general solution of Eq. (29), which is a second-order inhomogeneous linear differential equation, can be obtained by using the method of constant variation as

$$\begin{aligned} P_C^+(\alpha, y) = {} & B(\alpha)\cos\left[K(\alpha) y\right] + C(\alpha)\sin\left[K(\alpha) y\right] \\ & + \frac{1}{K(\alpha)} \int_0^y \left[f(\varsigma) + i\alpha g(\varsigma)\right] \sin\left[K(\alpha)(y - \varsigma)\right] d\varsigma, \end{aligned} \tag{32}$$

where $B(\alpha)$ and $C(\alpha)$ are unknown coefficients. Based on the transformed form of Eq. (5), Eq. (32) can be simplified into the following form:

$$\begin{aligned} P_C^+(\alpha, y) = B(\alpha)\left\{\cos\left[K(\alpha)y\right] + \frac{i\rho k c_0 \sin\left[K(\alpha)y\right]}{Z_2 K(\alpha)}\right\} \\ + \frac{1}{K(\alpha)}\int_0^y \left[f(\varsigma) + i\alpha g(\varsigma)\right]\sin\left[K(\alpha)(y-\varsigma)\right]d\varsigma \end{aligned}. \tag{33}$$

Combining the transformed pressure and particle velocity continuity relations at interface I and Eq. (28), we have

$$R^+(\alpha) = \frac{\partial}{\partial y}P_C^+(\alpha, L_y) - \frac{i\rho k c_0}{Z_4}P_C^+(\alpha, L_y). \tag{34}$$

Substituting Eq. (33) into Eq. (34) leads to

$$B(\alpha)W(\alpha) = R^+(\alpha) - \int_0^{L_y}\left[f(\varsigma) + i\alpha g(\varsigma)\right]\left\{\cos\left[K(\alpha)(L_y-\varsigma)\right] - \frac{i\rho k c_0 \sin\left[K(\alpha)(L_y-\varsigma)\right]}{Z_4 K(\alpha)}\right\}d\varsigma, \tag{35}$$

where

$$W(\alpha) = i\rho k c_0\left(\frac{1}{Z_2} - \frac{1}{Z_4}\right)\cos\left[K(\alpha)L_y\right] - \left[K^2(\alpha) - \frac{k^2\rho^2 c_0^2}{Z_2 Z_4}\right]\frac{\sin\left[K(\alpha)L_y\right]}{K(\alpha)}. \tag{36}$$

Substituting Eq. (35) into Eq. (33), we finally have the transformed sound pressure field of region C:

$$\begin{aligned} P_C^+(\alpha, y) = & \frac{\cos\left[K(\alpha)y\right] + \dfrac{i\rho k c_0 \sin\left[K(\alpha)y\right]}{Z_2 K(\alpha)}}{W(\alpha)} \\ & \times\left\{R^+(\alpha) - \int_0^{L_y}\left[f(\varsigma) + i\alpha g(\varsigma)\right]\left[\cos\left[K(\alpha)(L_y-\varsigma)\right] - \frac{i\rho k c_0 \sin\left[K(\alpha)(L_y-\varsigma)\right]}{Z_4 K(\alpha)}\right]d\varsigma\right\} \\ & + \frac{1}{K(\alpha)}\int_0^y \left[f(\varsigma) + i\alpha g(\varsigma)\right]\sin\left[K(\alpha)(y-\varsigma)\right]d\varsigma \end{aligned}. \tag{37}$$

Obviously, the term on the left-hand side (LHS) of Eq. (37) is a regular function in the upper half complex $\alpha$-plane. The regularity of the right-hand side (RHS) terms, however, is violated by the presence of the simple poles occurring at the zeros of the denominator lying in the upper half complex $\alpha$-plane satisfying

$$W\left(\alpha_m\right)=0, \quad m=0,1,2,\ldots. \tag{38}$$

These poles can be eliminated by imposing that their residues are zero, namely, the terms in the curly brace of Eq. (37) should be zero for each pole which gives

$$R^{+}\left(\alpha_m\right)=\int_0^{L_y}\left[f\left(\varsigma\right)+i\alpha_m g\left(\varsigma\right)\right]\left\{\cos\left[K\left(\alpha_m\right)\left(L_y-\varsigma\right)\right]-\frac{i\rho kc_0\sin\left[K\left(\alpha_m\right)\left(L_y-\varsigma\right)\right]}{Z_4K\left(\alpha_m\right)}\right\}d\varsigma\,. \tag{39}$$

Simplifying the terms in the curly brace of Eq. (39) by expanding the trigonometric functions and using Eq. (38), we have

$$\begin{aligned}R^{+}\left(\alpha_m\right)&=\left\{\cos\left[K\left(\alpha_m\right)L_y\right]-\frac{i\rho kc_0\sin\left[K\left(\alpha_m\right)L_y\right]}{Z_4K\left(\alpha_m\right)}\right\}\\&\times\int_0^{L_y}\left[f\left(\varsigma\right)+i\alpha_m g\left(\varsigma\right)\right]\left\{\cos\left[K\left(\alpha_m\right)\varsigma\right]+\frac{i\rho kc_0\sin\left[K\left(\alpha_m\right)\varsigma\right]}{Z_2K\left(\alpha_m\right)}\right\}d\varsigma\end{aligned}\,. \tag{40}$$

According to the form of the terms in the integrand of Eq. (40), we define two coefficients as

$$\begin{bmatrix}f_m\\g_m\end{bmatrix}=\frac{1}{N_m^C}\int_0^{L_y}\begin{bmatrix}f\left(y\right)\\g\left(y\right)\end{bmatrix}\left\{\cos\left[K\left(\alpha_m\right)y\right]+\frac{i\rho kc_0\sin\left[K\left(\alpha_m\right)y\right]}{Z_2K\left(\alpha_m\right)}\right\}dy\,. \tag{41}$$

Actually, the terms in the curly brace of Eq. (41) is the transversal modal function of region C:

$$Y_m^C\left(y\right)=\cos\left[K\left(\alpha_m\right)y\right]+\frac{i\rho kc_0\sin\left[K\left(\alpha_m\right)y\right]}{Z_2K\left(\alpha_m\right)}. \tag{42}$$

The normalized coefficient of the series expansion in Eq. (41) can be obtained by

$$N_m^C=\lim_{\alpha\to\alpha_m}\int_0^{L_y}Y^C\left(y\right)Y_m^C\left(y\right)dy=Y_m^C\left(L_y\right)\frac{dW\left(\alpha_m\right)}{2\alpha_m}. \tag{43}$$

Based on Eqs. (40) to (43), we have

$$R^{+}\left(\alpha_m\right)=\left\{\cos\left[K\left(\alpha_m\right)L_y\right]-\frac{i\rho kc_0\sin\left[K\left(\alpha_m\right)L_y\right]}{Z_4K\left(\alpha_m\right)}\right\}N_m^C\left[f_m+i\alpha_m g_m\right]. \tag{44}$$

Considering the transformed sound pressure continuity relation at the imaginary interface I and combining Eqs. (27) to (28), we have the following identity

$$P_C^{+}\left(\alpha,L_y\right)+P_A^{-}\left(\alpha,L_y\right)=\frac{iR^{+}\left(\alpha\right)}{K\left(\alpha\right)+\rho kc_0/Z_4}. \tag{45}$$

Substitute Eq. (37) into Eq. (45) and collect the like terms. Using the characteristics of the trigonometric functions, we have

$$\begin{aligned}&\frac{K\left(\alpha\right)+\rho kc_0/Z_2}{W\left(\alpha\right)e^{-iK(\alpha)L_y}\left[K\left(\alpha\right)+\rho kc_0/Z_4\right]}+P_A^{-}\left(\alpha,L_y\right)\\&=\frac{1}{W\left(\alpha\right)}\int_0^{L_y}\left[f\left(\varsigma\right)+i\alpha g\left(\varsigma\right)\right]\left\{\cos\left[K\left(\alpha_m\right)\varsigma\right]+\frac{i\rho kc_0\sin\left[K\left(\alpha_m\right)\varsigma\right]}{Z_2K\left(\alpha_m\right)}\right\}d\varsigma\end{aligned}. \tag{46}$$

Due to Eq. (41), we can express the defined functions in the form of series expansion as

$$\begin{bmatrix}f\left(y\right)\\g\left(y\right)\end{bmatrix}=\sum_{m=0}^{M}\begin{bmatrix}f_m\\g_m\end{bmatrix}Y_m^C\left(y\right), \tag{47}$$

where $M$ denotes the maximum number of truncated mode series. Substituting Eq. (47) into Eq. (46) and evaluating the resulting integral, we obtain a modified W-H equation of the second kind, which is valid in the shaded strip illustrated in Fig. 1, as

$$\frac{Z_4\chi\left(\eta_4,\alpha\right)R^{+}\left(\alpha\right)}{Z_2\chi\left(\eta_2,\alpha\right)N\left(\alpha\right)}+P_A^{-}\left(\alpha,L_y\right)=\sum_{m=0}^{M}\frac{f_m+i\alpha g_m}{\alpha^2-\alpha_m^2}Y_m^C\left(L_y\right), \tag{48}$$

where

$$\chi\left(\eta_z,\alpha\right)=\frac{K\left(\alpha\right)}{\eta_zK(\alpha)+k},\qquad \eta_z=Z_z/\rho c_0,\qquad z=2,4, \tag{49}$$

and

$$N(\alpha)=W(\alpha)e^{-iK(\alpha)L_y}. \tag{50}$$

Apparently, there are two unknowns $R^+(\alpha)$ and $P_A^-(\alpha,L_y)$ in Eq. (48). It seems that additional conditions are required in order to obtain the solutions. However, the impressive mathematical literature [21-26] proves that we can obtain the two unknowns at the same time by using the standard W-H procedures.

## 2.3 Solution of the W-H equation

To get the solutions of Eq. (48), split all the kernel functions into positive (+) and negative (-) parts which are regular and free of zeros in the upper and lower half complex α-plane, respectively as

$$\begin{aligned}&\frac{Z_4\chi^+(\eta_4,\alpha)\chi^-(\eta_4,\alpha)R^+(\alpha)}{Z_2\chi^+(\eta_2,\alpha)\chi^-(\eta_2,\alpha)N^+(\alpha)N^-(\alpha)}+P_A^-(\alpha,L_y)\\&=\sum_{m=0}^{M}\left[\frac{f_m+i\alpha_m g_m}{2\alpha_m(\alpha-\alpha_m)}-\frac{f_m-i\alpha_m g_m}{2\alpha_m(\alpha+\alpha_m)}\right]Y_m^C(L_y)\end{aligned}. \tag{51}$$

The explicit expression of the split function $N^+(\alpha)$ can be obtained according to the method described by Mittra [29] as

$$\begin{aligned}N^+(\alpha)=&\sqrt{i\rho kc_0\left(\frac{1}{Z_2}-\frac{1}{Z_4}\right)\cos(kL_y)-k\left(1-\frac{\rho^2c_0^2}{Z_2Z_4}\right)\sin(kL_y)}\\&\times\exp\left\{\frac{K(\alpha)L_y}{\pi}\ln\left[\frac{\alpha-iK(\alpha)}{k}\right]-\frac{i\alpha L_y}{\pi}\left[1-C+\ln\left(\frac{2\pi}{kL_y}\right)-\frac{i\pi}{2}\right]\right\}\prod_{m=1}^{L}\left(1+\frac{\alpha}{\alpha_m}\right)e^{\left(\frac{-i\alpha L_y}{m\pi}\right)},\end{aligned} \tag{52}$$

where $C$ is the Euler-Mascheroni constant, which is given by $C$=0.5772 ... and $L$ is the maximum split number. Similarly, the factorization of $\chi(\eta_z,\alpha)$ can be written in terms of Maluizhinets function as

$$\chi^{-}\left(\eta_z, k\cos\phi\right) = \frac{4\left[M_\pi\left(\frac{3\pi}{2}-\phi-\theta\right)M_\pi\left(\frac{\pi}{2}-\phi+\theta\right)\right]^2\sin\left(\frac{\phi}{2}\right)}{\sqrt{\eta_z}\left[M_\pi\left(\frac{\pi}{2}\right)\right]^4\left[1+\sqrt{2}\cos\left(\frac{3\pi-2\phi-2\theta}{4}\right)\right]\left[1+\sqrt{2}\cos\left(\frac{\pi-2\phi+2\theta}{4}\right)\right]}, \quad z=2,4. \tag{53}$$

The Maluizhinets function is defined as

$$M_\pi\left(v\right) = \exp\left\{-\frac{1}{8\pi}\int_0^v \frac{1}{\cos u}\left[\pi\sin u - 2\sqrt{2}\pi\sin\left(\frac{u}{2}\right) - 2u\right]du\right\}, \tag{54}$$

with

$$\sin\theta = \frac{1}{\eta_z}, \quad z=2,4. \tag{55}$$

The split functions have the following characteristics:

$$N^{+}\left(\alpha\right) = N^{-}\left(-\alpha\right), \tag{56}$$

$$\chi^{+}\left(\eta_z, k\cos\phi\right) = \chi^{-}\left(\eta_z, -k\cos\phi\right), \quad z=2,4. \tag{57}$$

Collecting the terms which are regular in the upper half complex $\alpha$-plane at the LHS and those regular in the lower half complex $\alpha$-plane at the RHS, then we have

$$\begin{aligned}&\frac{Z_4\chi^{+}\left(\eta_4,\alpha\right)R^{+}\left(\alpha\right)}{Z_2\chi^{+}\left(\eta_2,\alpha\right)N^{+}\left(\alpha\right)} + \sum_{m=0}^{M} Y_m^C\left(L_y\right)\frac{f_m - i\alpha_m g_m}{2\alpha_m\left(\alpha+\alpha_m\right)}\frac{\chi^{-}\left(\eta_2,\alpha\right)N^{-}\left(\alpha\right)}{\chi^{-}\left(\eta_4,\alpha\right)} \\ &= \sum_{m=0}^{M} Y_m^C\left(L_y\right)\frac{f_m + i\alpha_m g_m}{2\alpha_m\left(\alpha-\alpha_m\right)}\frac{\chi^{-}\left(\eta_2,\alpha\right)N^{-}\left(\alpha\right)}{\chi^{-}\left(\eta_4,\alpha\right)} - P_A^{-}\left(\alpha, L_y\right)\frac{\chi^{-}\left(\eta_2,\alpha\right)N^{-}\left(\alpha\right)}{\chi^{-}\left(\eta_4,\alpha\right)}\end{aligned}. \tag{58}$$

The second term on the LHS of Eq. (58) has singularities at the zeros of the denominator which can be decomposed and then isolated with the help of Cauchy formula in the following manner

$$\begin{aligned}
&\frac{Z_4\chi^+(\eta_4,\alpha)R^+(\alpha)}{Z_2\chi^+(\eta_2,\alpha)N^+(\alpha)}+\sum_{m=0}^{M}Y_m^C(L_y)\frac{f_m-i\alpha_m g_m}{2\alpha_m(\alpha+\alpha_m)}\frac{\chi^-(\eta_2,-\alpha_m)N^-(-\alpha_m)}{\chi^-(\eta_4,-\alpha_m)}\\
&+\sum_{m=0}^{M}Y_m^C(L_y)\frac{f_m-i\alpha_m g_m}{2\alpha_m(\alpha+\alpha_m)}\left[\frac{\chi^-(\eta_2,\alpha)N^-(\alpha)}{\chi^-(\eta_4,\alpha)}-\frac{\chi^-(\eta_2,-\alpha_m)N^-(-\alpha_m)}{\chi^-(\eta_4,-\alpha_m)}\right]\\
&=\sum_{m=0}^{M}Y_m^C(L_y)\frac{f_m+i\alpha_m g_m}{2\alpha_m(\alpha-\alpha_m)}\frac{\chi^-(\eta_2,\alpha)N^-(\alpha)}{\chi^-(\eta_4,\alpha)}-P_A^-(\alpha,L_y)\frac{\chi^-(\eta_2,\alpha)N^-(\alpha)}{\chi^-(\eta_4,\alpha)}
\end{aligned}. \tag{59}$$

Making full use of the properties of split functions listed in Eq. (56) and Eq. (57) and taking into consideration the analytical continuation principle obeying the Liouville's theorem, the solution of Eq. (59) can be obtained:

$$R^+(\alpha)=-\frac{Z_2\chi^+(\eta_2,\alpha)N^+(\alpha)}{Z_4\chi^+(\eta_4,\alpha)}\sum_{m=0}^{M}Y_m^C(L_y)\frac{f_m-i\alpha_m g_m}{2\alpha_m(\alpha+\alpha_m)}\frac{\chi^+(\eta_2,\alpha_m)N^+(\alpha_m)}{\chi^+(\eta_4,\alpha_m)}. \tag{60}$$

## 2.4 Sound fields in the natural domain

As can be observed, Eq. (60) contains an infinite number of unknown coefficients. To determine these coefficients, we apply the well-known mode-matching technique, which has been extensively applied to analyze the sound field in waveguide structures. Combining Eqs. (8), (10) and (30), we have

$$\begin{aligned}
&f(y)\pm i\alpha g(y)=\frac{\partial p_C(0,y)}{\partial x}\pm i\alpha p_C(0,y)\\
&=\frac{\partial}{\partial x}\left[p_B^{inc}(0,y)+p_B(0,y)\right]\pm i\alpha\left[p_B^{inc}(0,y)+p_B(0,y)\right]
\end{aligned}. \tag{61}$$

Substituting Eqs. (47), (15) and (20) into Eq. (61), we have the following identity

$$\begin{aligned}
&\sum_{m=0}^{M}(f_m\pm i\alpha g_m)Y_m^C(y)\\
&=-\frac{i\rho kc_0Q_0}{2}\sum_{n=0}^{N}\frac{(\phi_n\mp\alpha)Y_n^B(y_0)Y_n^B(y)e^{i\phi_n x_0}}{N_n^B\phi_n}+\sum_{j=0}^{J}ib_j(\phi_j\pm\alpha)Y_j^B(y)
\end{aligned}. \tag{62}$$

Multiply both sides of Eq. (62) by modal function $Y_s^C(y)$ and conduct the integration over the opening in terms of $y$ from zero to $L_y$. Then, using the orthogonality of modal functions, one obtains

$$f_s \pm i\alpha g_s = -\frac{i\rho k c_0 Q_0}{2}\sum_{n=0}^{N}\frac{\left(\phi_n \mp \alpha\right)Y_n^B\left(y_0\right)e^{i\phi_n x_0}\Delta_{ns}}{N_s^C N_n^B \phi_n} + \sum_{j=0}^{J}\frac{ib_j\left(\phi_j \pm \alpha\right)\Delta_{js}}{N_s^C}, \tag{63}$$

where

$$\Delta_{j(n)s} = \frac{i\rho k c_0\left(\dfrac{1}{Z_1}-\dfrac{1}{Z_2}\right)}{\xi_{j(n)}^2 - K^2\left(\alpha_s\right)} + \frac{i\rho k c_0\left(\dfrac{1}{Z_3}+\dfrac{1}{Z_4}\right)}{\xi_{j(n)}^2 - K^2\left(\alpha_s\right)}Y_{j(n)}^B\left(L_y\right)Y_s^C\left(L_y\right). \tag{64}$$

Combining the W-H solution $R^+\left(\alpha\right)$ and the residue solution $R^+\left(\alpha_m\right)$, they should be equal at a specific value $\alpha_s$. Then we have the following equation

$$\begin{aligned}&\left\{\cos\left[K\left(\alpha_s\right)L_y\right] - \frac{i\rho k c_0 \sin\left[K\left(\alpha_s\right)L_y\right]}{Z_4 K\left(\alpha_s\right)}\right\}N_s^C\left(f_s + i\alpha_s g_s\right)\\ &= -\frac{Z_2\chi^+\left(\eta_2,\alpha_s\right)N^+\left(\alpha_s\right)}{Z_4\chi^+\left(\eta_4,\alpha_s\right)}\sum_{m=0}^{M}Y_m^C\left(L_y\right)\frac{f_m - i\alpha_m g_m}{2\alpha_m\left(\alpha_s+\alpha_m\right)}\frac{\chi^+\left(\eta_2,\alpha_m\right)N^+\left(\alpha_m\right)}{\chi^+\left(\eta_4,\alpha_m\right)}\end{aligned}. \tag{65}$$

Substituting Eqs. (63) and (64) into Eq. (65), finally, we have

$$\sum_{j=0}^{J}A_j\left(\alpha_s\right)b_j = \Phi\left(\alpha_s\right), \tag{66}$$

where

$$\begin{aligned}A_j\left(\alpha_s\right) &= \left(\phi_j + \alpha_s\right)\Delta_{js}\left\{\cos\left[K\left(\alpha_s\right)L_y\right] - \frac{i\rho k c_0 \sin\left[K\left(\alpha_s\right)L_y\right]}{Z_4 K\left(\alpha_s\right)}\right\}\\ &+ \frac{Z_2}{Z_4}\frac{\chi^+\left(\eta_2,\alpha_s\right)N^+\left(\alpha_s\right)}{\chi^+\left(\eta_4,\alpha_s\right)}\sum_{m=0}^{M}Y_m^C\left(L_y\right)\frac{\left(\phi_j - \alpha_m\right)\Delta_{jm}}{2N_m^C\alpha_m\left(\alpha_s+\alpha_m\right)}\frac{\chi^+\left(\eta_2,\alpha_m\right)N^+\left(\alpha_m\right)}{\chi^+\left(\eta_4,\alpha_m\right)}\end{aligned}, \tag{67}$$

and

$$\begin{aligned}\Phi\left(\alpha_s\right) &= \frac{\rho k c_0 Q_0}{2}\sum_{n=0}^{N}\left(\phi_n - \alpha_s\right)\frac{Y_n^B\left(y_0\right)e^{i\varphi_n x_0}\Delta_{ns}}{N_n^B\phi_n}\left\{\cos\left[K\left(\alpha_s\right)L_y\right] - \frac{i\rho k c_0 \sin\left[K\left(\alpha_s\right)L_y\right]}{Z_4 K\left(\alpha_s\right)}\right\}\\ &+ \frac{\rho k c_0 Q_0 Z_2}{4Z_4}\frac{\chi^+\left(\eta_2,\alpha_s\right)N^+\left(\alpha_s\right)}{\chi^+\left(\eta_4,\alpha_s\right)}\sum_{m=0}^{M}Y_m^C\left(L_y\right)\frac{\sum_{n=0}^{N}\dfrac{\left(\phi_n + \alpha_m\right)Y_n^B\left(y_0\right)e^{i\phi_n x_0}\Delta_{nm}}{N_n^B\phi_n}}{N_m^C\alpha_m\left(\alpha_s+\alpha_m\right)}\frac{\chi^+\left(\eta_2,\alpha_m\right)N^+\left(\alpha_m\right)}{\chi^+\left(\eta_4,\alpha_m\right)}\end{aligned}. \tag{68}$$

Rewrite Eq. (66) in matrix form

$$\boldsymbol{A}\boldsymbol{b} = \boldsymbol{\Phi}, \tag{69}$$

where

$$\boldsymbol{A} = \begin{bmatrix} A_0(\alpha_0) & A_1(\alpha_0) & \cdots & A_J(\alpha_0) \\ A_0(\alpha_1) & A_1(\alpha_1) & \cdots & A_J(\alpha_1) \\ \vdots & \vdots & \vdots & \vdots \\ A_0(\alpha_s) & A_1(\alpha_s) & \ldots & A_J(\alpha_s) \end{bmatrix}, \quad \boldsymbol{b} = \begin{bmatrix} b_0 \\ b_1 \\ \vdots \\ b_J \end{bmatrix}, \quad \boldsymbol{\Phi} = \begin{bmatrix} \Phi(\alpha_0) \\ \Phi(\alpha_1) \\ \vdots \\ \Phi(\alpha_s) \end{bmatrix}. \tag{70}$$

The modal response coefficients $\boldsymbol{b}$ can be obtained by solving Eq. (69) numerically. Then, the sound field inside a long enclosure can be determined. The radiated sound pressure field of region A in the natural domain can be obtained by taking the inverse Fourier transform of Eq. (27) as

$$p_A(x,y) = \frac{1}{2\pi}\int_{\Gamma} \frac{iR^+(\alpha)}{K(\alpha)+\rho k c_0/Z_4} e^{-iK(\alpha)(y-L_y)+i\alpha x} d\alpha . \tag{71}$$

Here, the integration path Γ is a straight line along the real axis lying in the common strip of the upper and lower complex α-planes as shown in Fig. 2. To perform an asymptotic evaluation of Eq. (71) through the saddle point method, we perform a change of variables into cylindrical coordinates as

$$\alpha = -k\cos w, \quad x = r\cos\theta, \quad y = r\sin\theta . \tag{72}$$

Then, Eq. (71) becomes

$$p_A(r,\theta) = \frac{1}{2\pi}\int_{\Gamma_w} \frac{iR^+(-k\cos w)k\sin w e^{-ik\sin w L_y}}{\rho k c_0/Z_4 - k\sin w} e^{krg(w)} dw, \tag{73}$$

with

$$g(w) = -i\cos(w+\theta), \tag{74}$$

where the new integration contour $\Gamma_w$ in the complex w-plane is illustrated by the solid blue arrow line in Fig. 3. Next, we deform the path into a new path $\Gamma_s$ known as the steepest descent path (SDP) which passes

through the saddle point $w = -\theta$. The criteria for the selection of $\Gamma_s$ are that the imaginary part of g(w) is constant and its real part reaches the maximum value at the saddle point.

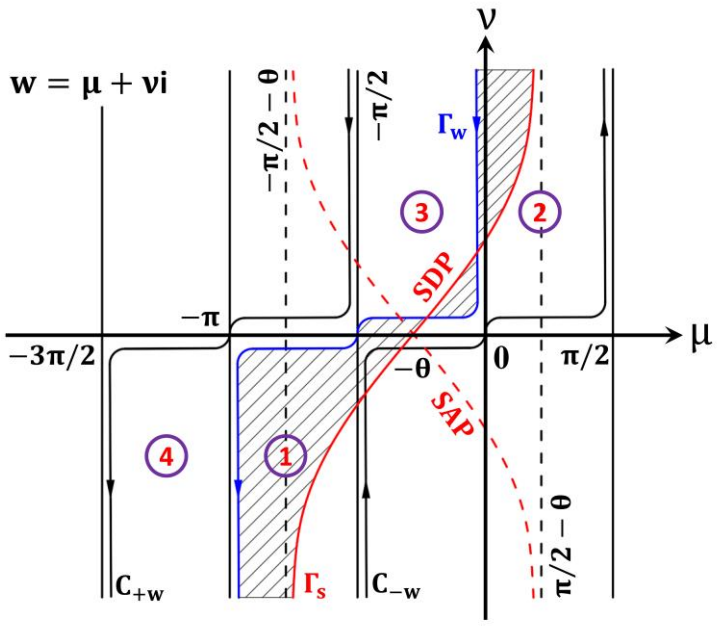


Fig. 3. Sketch of mapping $\alpha = -k\cos w$ from the complex $\alpha$-plane to the complex w-plane. Integration path $\Gamma_w$ (solid blue arrow line), the steepest descent path $\Gamma_s$ (SDP, solid red line), the steepest ascent path (SAP, dashed red line), the four quadrants of the proper sheet (red numbers with purple circles) and the branch cuts $C_{\pm w}$ (dark solid arrow lines) are presented.

As $kr \to \infty$, the major contribution to the integral of Eq. (73) along $\Gamma_s$ comes from a small segment around the saddle point due to the exponentially decaying factor in the integrand. Making full use of the error integral, the asymptotic evaluation of Eq. (73) along the SDP through the saddle point method gives

$$p_A(r,\theta) = \frac{ik\sin\theta e^{ik\sin\theta L_y} e^{-ikr} e^{\frac{\pi}{4}i}}{\sqrt{2\pi kr}\left[k\sin\theta + \rho k c_0 / Z_4\right]} R^+\left(-k\cos\theta\right) \cdot \tag{75}$$

To obtain an accurate result, sufficient truncation number should be determined first. Detailed information will be given in section 3.

# 3. Results and discussions

In this section, numerical simulations are carried out to examine the correctness and accuracy of the proposed model. In theory, the size of the acoustical domain, boundary conditions and targeted frequency range can be arbitrary. For the sake of calculation efficiency, we start with a relatively small enclosure whose height is 1 m and length is 5 m. The boundary conditions applied to the wall and ground surfaces come from different kinds of liners which have been thoroughly introduced in [30]. Their acoustic impedances are $Z_1$=202+13i, $Z_2$=1840+370i, $Z_3$=458+517i and $Z_4$=630-651i. In addition, a monopole point source with its volume velocity strength being $Q_0$=0.01 $m^2/s$ is located at (-2, 0.2) m. In this paper, the sound speed and the density of air are 343 m/s and 1.225 $kg/m^3$, respectively.

## 3.1 Targeted frequency range

Before conducting the calculations, a preliminary experiment was performed to determine the basic properties of traffic noise outside a tunnel in Hong Kong. According to the measurement method described in the environmental quality standard for noise (GB 3096-2008), day-time equivalent A-weighted SPLs at different locations were obtained by a sound level meter (Larson Davis Model 831). Their average value reached 78 dB (A) and exceeded the threshold specified in the standard which is 70 dB (A) for urban arterial roads. Also, the measured SPL spectra of the average noise radiated from the tunnel with stable traffic flow, from buses and heavy trucks traveling at approximately 70 km/h are presented in Fig. 4. Apart from the fluctuating results under around 200 Hz which may due to the random vibration or the limitation of our equipment, the noise energy is concentrated mainly in the frequency range of 200 Hz to 2000 Hz. For the higher-frequency intervals, however, the SPLs decrease continuously and dissipate quite easily in the open space with increasing distance. According to our main purpose of predicting the far-field

directivity pattern of the radiated sound field, we focus on the frequency range of 200 Hz to 2000 Hz in the following research.

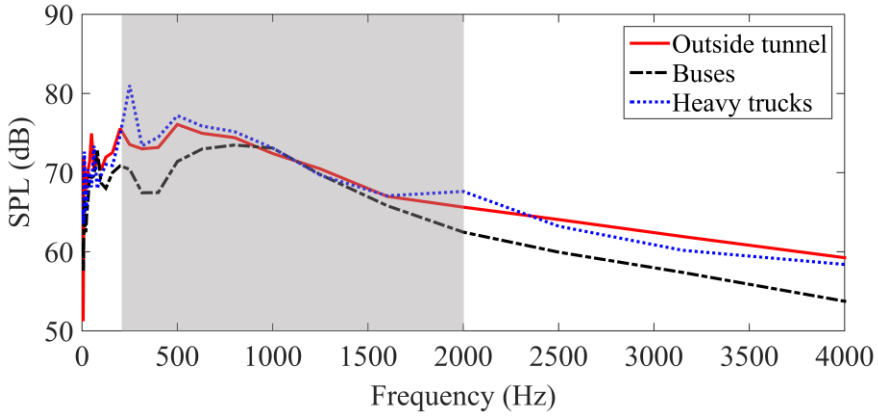


Fig. 4. Measurement SPL spectra of the average noise radiated from a tunnel with stable traffic flow, from buses and heavy trucks traveling at about 70 km/h.

## 3.2 Calculation of the wavenumbers

As the representation of sound field inside the enclosure is based on mode theory, a correct solution to the problem requires a successful determination of the wavenumbers both in regions B and C, which are defined by Eqs. (17) and (38), respectively. To find the roots of these characteristic equations, the classical Newton-Raphson method can be applied, but care should be taken in selecting the proper initial values and step length to implement the iteration scheme. Fortunately, the roots are symmetric about the origin with certain periodicity due to the nature of trigonometric functions, which can reduce the time cost during the calculation. However, one thing that should be bear in mind is that the period does not start from the first root and it exists only in either the real or the imaginary parts of the roots. Knowing this, we start the iteration from zero and define a step length that is slightly smaller than the period, which can be determined by a pilot calculation. Taking 1000 Hz as an example, a small fraction of wavenumbers along horizontal and transversal directions in regions B and C are listed in Fig. 5. As can be seen in Fig. 5 (a), the first root of Eq. (38) is 17.68-0.13i. It is quite close to the free space wavenumber which is 18.32 but has a certain

deviation and imaginary part due to the impedance boundary conditions. In addition, the imaginary parts of these roots stably decrease over $2\pi$ and finally tend to $-\infty$. The real parts decrease as well but eventually converge to zero. In Fig. 5 (b), on the contrary, the real parts of the roots have a period of $2\pi$ and finally tend to $+\infty$, however, the imaginary parts decrease steadily and ultimately converge to zero. Similar patterns can be observed in Fig. 5 (c) and Fig. 5 (d), but the rates of change are different due to different boundary conditions. These principles apply to other frequencies as well and will not be elaborated.

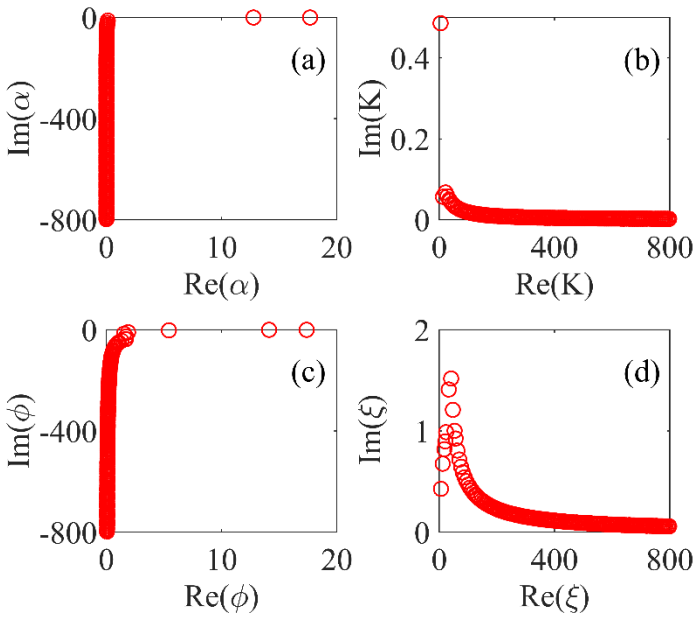


Fig. 5. The horizontal (a, c) and the transversal (b, d) wavenumbers of regions C and B at 1000 Hz obtained by the classical Newton-Raphson method.

The wavenumbers of region B are used for the superposition of normal modes. For the size of the geometry and frequency range at hand, 100 modes are obtained. However, the wavenumbers of region C are mainly for the calculation of the split function in Eq. (52). To guarantee the convergence of this calculation, 5000 pairs of roots are prepared. With these preparations, the sound fields inside and outside the long enclosure can be determined immediately. We highlight that an advantage of the proposed method is that, for long

enclosures with the same size and boundary conditions, the obtained wavenumbers can be reused to explore the properties of sound fields in other situations, including different source locations and different kinds of incident waves. Therefore, the time spent on similar calculations by numerical methods can be reduced by the W-H technique.

### 3.3 Model validation through the FEM

As the incident and reflected sound fields inside the long enclosure share the same modal function, the number of modes used in the calculations should be determined first. A convergence check is carried out to find out the maximum mode number based on a trade-off between computation cost and accuracy. The criterion of convergence is defined that the relative error of pressure values between two successive mode numbers at arbitrary location is less than 1%. Because the maximum mode number would increase as the increase of dimension and frequency. The maximum mode number could be obtained by examining the convergence of the total sound pressure of arbitrarily picked point (-1, 0.7) m at 2000 Hz. As presented in Fig. 6, the real and imaginary parts of sound pressure become stable after about 12 modes with the split number being 500.

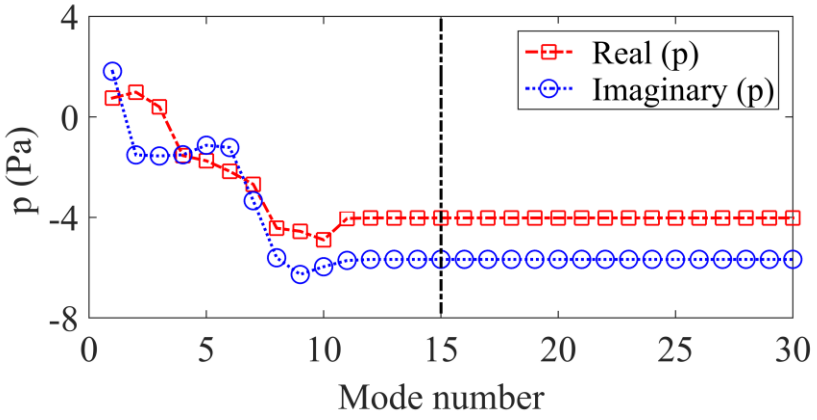


Fig. 6. Convergence analysis of the total sound pressure field of receiver point (-1, 0.7) m at 2000 Hz.

Then, a comparison of the total sound pressure fields in region B obtained by the FEM and the W-H technique at 2000 Hz is conducted. The commercial software COMSOL Multiphysics is applied for the FEM. In the proposed method, the size of the enclosure and outside region can be infinite. However, this is impossible for the FEM. To solve this problem, the calculation domain is bounded by a PML, which is an artificial absorption layer that allows sound wave to propagate out without any reflections [31]. To ensure the accuracy of the FEM and to satisfy the basic requirement for the acoustic mesh which states that the maximum side-length of acoustic element should be less than 1/6 of the minimum wavelength in targeted frequency range, the acoustic domain is discretized into more than $6.5\times10^5$ elements with dimensions below 0.01 m. In addition, both the curvature parameter and scaling factor of the PML are set to be 1 in the current analysis according to the findings by Hein, Hohage and Koch [32]. As presented in Fig. 7, good agreement can be found. Despite the fact that discrepancies exist, they differ from each other with a relative error much less than 1%, which might be caused by mathematical issues.

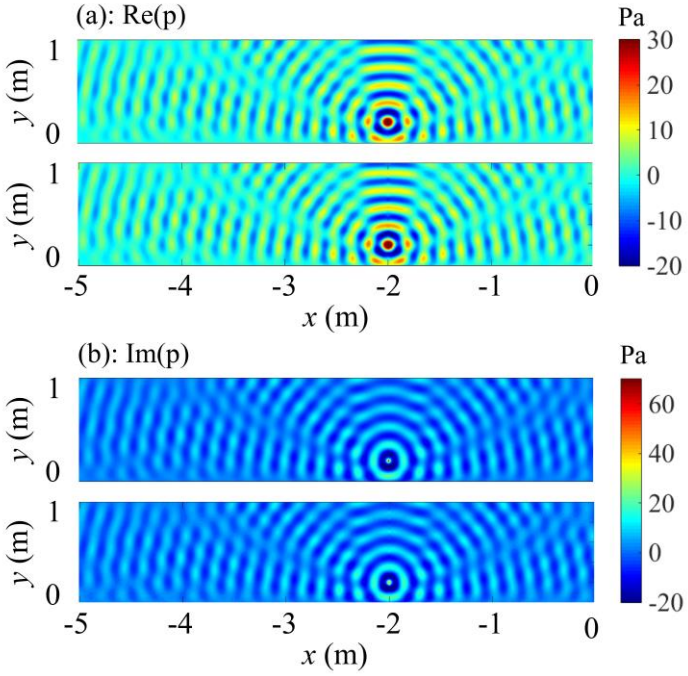

Fig. 7. A comparison of real (a) and imaginary (b) parts of the total sound pressure field in region B calculated by the FEM (first row) and the W-H technique (second row).

After several tentative calculations, finally, a split number of 500 is used in Eq. (52), and 15 modes are taken into account in Eqs. (15) and (20) for this configuration to ensure the accuracy. The results indicate that the split and modal number are sufficient as a further increase in these numbers does not produce a significant difference in this study. Comparisons between the SPLs obtained by the W-H technique and the FEM in the targeted frequency range at randomly picked receiver points are illustrated in Fig. 8. Good agreement can be observed, which validates the correctness and accuracy of the proposed prediction model in the calculation of sound field inside an enclosure.

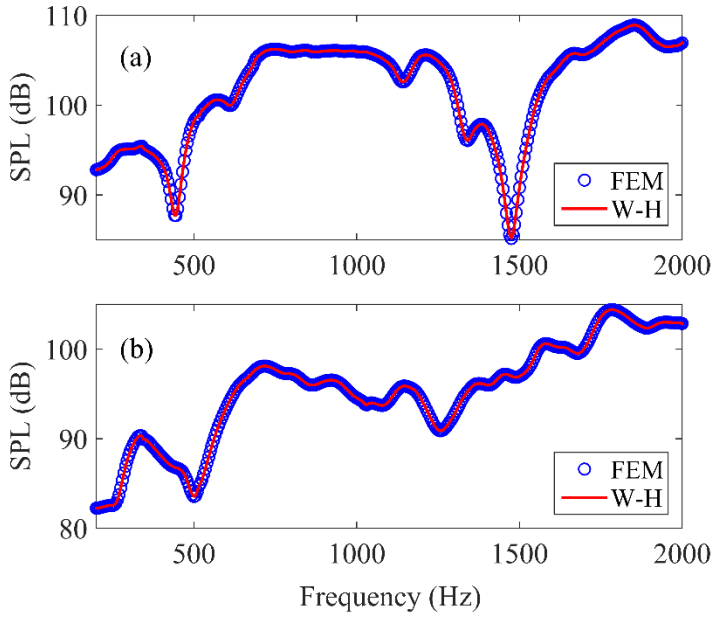


Fig. 8. SPL spectra in the targeted frequency range obtained by the W-H technique and the FEM at different receivers inside the long enclosure: (a) receiver (-1, 0.7) m, (b) receiver (-5, 0.3) m.

The directivity patterns of the radiated sound fields outside the long enclosure at different frequencies obtained by the W-H technique and the FEM are presented in a polar coordinate system as shown in Fig. 9. The results coincide well with each other even though there are some discrepancies, which may result from the far-field approximation. In front of the opening, the lobes can be clearly seen, and the number of lobes increases with increasing frequency. This part of sound field is formed by the superposition of direct, diffracted and reflected sound waves. These waves propagate to the receiver over different distance and with different phases, which results in the directivity pattern. At the backside of the enclosure, the sound field is the result of diffraction at the opening edge which, according to the GTD, is mainly determined by the incident and diffracted angles and the distance between the source and the receiver. This part of sound field is quite stable and standing at a relatively low SPL. Based on these features, we can smooth and manipulate the angle of the lobes in front of the opening and attenuate the diffracted sound at the backside of the enclosure to control the radiated noise.

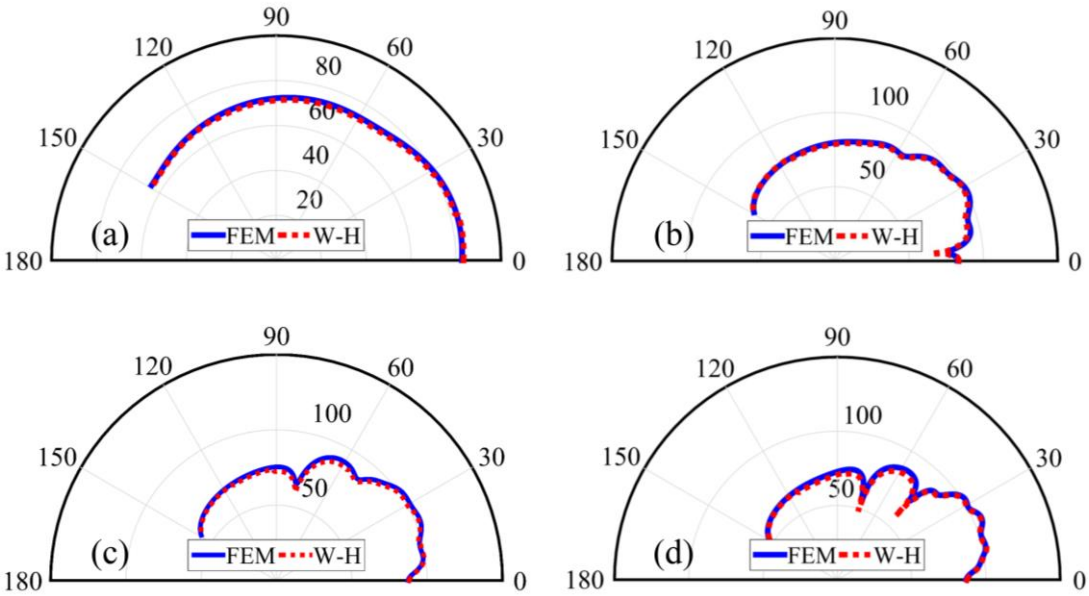


Fig. 9. Directivity patterns of the radiated SPLs (dB) obtained by the W-H technique and the FEM when distance r = 3 m at specific frequencies: (a) 200 Hz, (b) 900 Hz, (c) 1600 Hz, (d) 2000 Hz.

From the results presented in the preceding content, the W-H technique is capable of predicting the sound fields both inside and outside a long enclosure with a certain accuracy. To verify the capability of the proposed method to handle a large-size geometry, larger enclosures are considered sequentially. The results obtained using the W-H technique and the FEM are consistent and are not presented here. The main difference is the calculation time.

Tab. 1. Comparison of calculation time between W-H technique and the FEM in different configurations.

| Configuration [m] | | | | W-H technique | | | FEM | |
|---|---|---|---|---|---|---|---|---|
| Height | Length | Radius | | Modes | Time [h] | | Elements | Time [h] |
| 0.5 | 2.5 | 3 | | 10 | 1.13 | | $1.6\times10^5$ | 1.07 |
| 1 | 5 | 6 | | 15 | 3.61 | | $6.5\times10^5$ | 5.32 |
| 2 | 7 | 8 | | 20 | 6.82 | | $1.7\times10^6$ | 13.2 |
| 5 | 10 | 12 | | 30 | 23.3 | | $3.7\times10^6$ | 28.7 |

As shown in Tab. 1, for small acoustic domain, the calculation time required by the W-H technique and the FEM are roughly the same. With an increase in the size of the geometry, more modes and split numbers should be taken into consideration in order to obtain an accurate result when using the W-H technique. Accordingly, its calculation efficiency will reduce to some extent. Fortunately, it is easy for computers to perform summations so that the calculation efficiency in big size condition is still acceptable. Furthermore, the calculation efficiency of the radiated field is not constrained by the size of the outside domain because it is an explicit expression in terms of distance. However, for the FEM, the element number grows rapidly with an increase in the size of the geometry. This will lead to low efficiency, particularly in the case of real traffic facilities. Thus, under such big size condition, the W-H technique performs better than the FEM, especially when far-field results are required in engineering applications.

## 3.4 Potential noise control strategies by using acoustic liners

Acoustic liners [33-35] are widely used to attenuate noise in ducted systems. Combining Eqs. (60), (63) and (75), we notice that the radiated sound field is determined by the incident and reflected sound inside the long enclosure. Hence, the radiated noise can be reduced through the control of the sound field inside the enclosure. To verify this conjecture and provide some data to support the proposal of noise control strategies, three cases with different boundary conditions (liners introduced in [30]), namely, totally rigid, only an impedance $Z_3$ on the inner wall, and all the surfaces having impedances $Z_1$~$Z_4$, are analyzed thoroughly. In these cases, the monopole point source is located at (-2, 0.5) m, and the height of the long enclosure is 2 m. The SPL spectra for a receiver (-1, 1) m inside the enclosure are presented in Fig. 10. Several peaks occur at the resonance frequencies [27] of the enclosure in the totally rigid case, which indicates that the sound field inside the enclosure strongly depends on the height. Taking the rigid case as the basis, the introduction of liners on the boundaries can significantly reduce the SPL over most of the frequency range, which is determined by the resistance and reactance provided by the acoustic impedance. However, the effects of the impedance values and the number of liners cannot be clearly reflected in this figure and will be considered in the future.

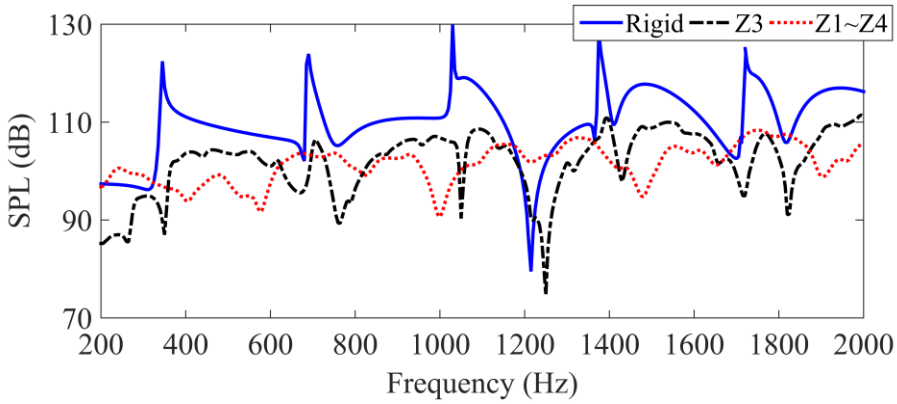


Fig. 10. SPL spectra under different boundary conditions for a receiver (-1, 1) m inside a long enclosure with its height being 2 m.

Furthermore, the directivity patterns of the radiated sound fields at specific frequencies are presented in Fig. 11. Compared to the rigid case, the introduction of liners on the boundaries can reduce the SPL of the radiated sound field between the observation angles of 60~150 degrees, and in general, the case in which all surfaces have impedances reduces the SPL more than the case with only $Z_3$. However, between 0~60 degrees, the reduction becomes blurred as the SPLs vary irregularly. Besides, some dips in the rigid case disappear after introducing the impedance. Despite this, the lobes in the rigid case are more or less smoothed in the impedance cases, which is significant for controlling noise. Another phenomenon in the rigid case that deserves attention is that, between the observation angles of 60~90 degrees, there will always be one or more lobes with SPLs standing at relatively high levels. These lobes are the so-called principal lobes and will be our focus of consideration in proposing noise control strategies.

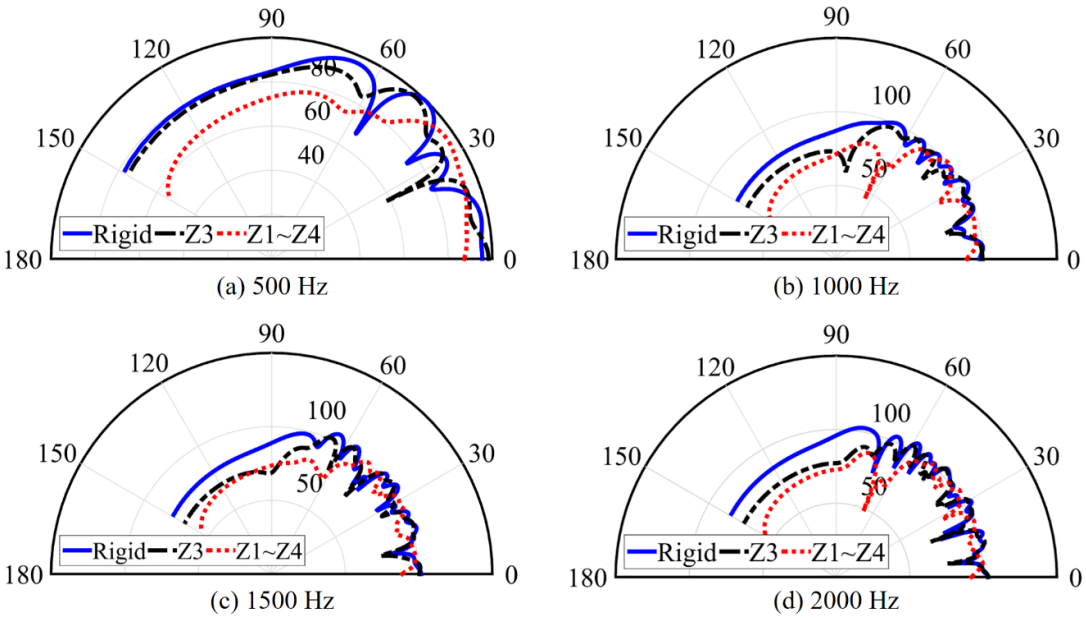


Fig. 11. Directivity patterns of the radiated sound fields under different boundary conditions and at specific frequencies: (a) 500 Hz, (b) 1000 Hz, (c) 1500 Hz, (d) 2000 Hz.

According to the foregoing analysis, it is practicable to control the noise both inside and outside the long enclosure by using acoustic liners. In practical applications, however, the ground is not convenient for the introduction of noise reduction structures and is usually considered to be totally rigid [36]. Besides, the length of these linings should be finite which is less costly and more realistic. From the result of case with only $Z_3$ presented above, the noise reduction is not as good as expected. Therefore, the design of the location, length and optimized value of the impedance on the wall of the enclosure will be studied in the future. On the other hand, in this paper, liners with constant impedances are used mainly to validate the proposed model and examine their potential to attenuate noise inside and outside a long enclosure. Currently, with the development of acoustic metamaterials, new types of liners [37] that can provide inhomogeneous impedances [31, 38] are widely used for reflection wave manipulation and noise attenuation purposes. These structures have great potential for the control of noise inside and outside long enclosures.

# 4. Conclusions

In this paper, a rigorous and explicit model is established for the prediction of sound radiated from a semi-infinite long enclosure, in which an unbaffled opening, the ground effect and a point source excitation are taken into consideration simultaneously in order to model practical traffic facilities. The results obtained by the W-H technique and the FEM are compared and discussed, which indicates that the proposed method is capable of predicting the sound fields both inside and outside a long enclosure with high accuracy and efficiency.

The advantages of the W-H technique over the FEM are summarized as follows: 1). for enclosures with identical configurations, the obtained wavenumbers can be reused which avoids excessive calculation time for similar calculations; 2). the proposed model can be applied to a broad frequency range and generalized to arbitrary boundary conditions. In addition, there is no size restriction for the proposed model.

The performance of acoustic liners with constant impedances in attenuating the noise inside and outside a long enclosure is investigated, based on which potential noise reduction approaches are introduced. The proposed model will be an effective tool for conducting parameter studies, explaining the physics behind radiation phenomenon and proposing appropriate noise control strategies.

## Acknowledgements

The authors would like to acknowledge the funding from The Hong Kong Polytechnic University (PolyU152029/17E) and (PolyU152666/16E). The first author would like to thank the studentship provided by The Hong Kong Polytechnic University.

## References


[1] J. Kang, Reverberation in rectangular long enclosures with geometrically reflecting boundaries, Acta Acust. United Acust. 82 (3) (1996) 509-516.

[2] J. Kang, Acoustics in long enclosures with multiple sources, J. Acoust. Soc. Am. 99 (2) (1996) 985-989.

[3] K. Heutschi, R. Bayer, Sound radiation from railway tunnel openings, Acta Acust. United Acust. 92 (4) (2006) 567-573.

[4] P. E. Doak, Excitation, transmission and radiation of sound from source distributions in hard-walled ducts of finite length (i): the effects of duct cross-section geometry and source distribution space-time pattern, J. Sound Vib. 31 (1) (1973) 1-72.

[5] K. M. Li, K. K. Iu, Propagation of sound in long enclosures, J. Acoust. Soc. Am. 116 (5) (2004) 2759-2770.

[6] P. M. Lam, K. M. Li, A coherent model for predicting noise reduction in long enclosures with impedance discontinuities, J. Sound Vib. 299 (3) (2007) 559-574.

[7] H. Min, W. Chen, X. Qiu, Single frequency sound propagation in flat waveguides with locally reactive impedance boundaries, J. Acoust. Soc. Am. 130 (2) (2011) 772-782.

[8] A. McAlpine, A. P. Daymond-King, A. J. Kempton, Sound radiation from a flanged inclined duct, J. Acoust. Soc. Am. 132 (6) (2012) 3637-3646.

[9] A. D. Pierce, Acoustics: An Introduction to its Physical Principles and Applications, McGraw-Hill, New York, 1981, pp. 213–215.

[10] H. Levine, J. Schwinger, On the radiation of sound from an unflanged circular pipe, Phys. Rev. 73 (4) (1948) 383-406.

[11] J. Lordi, G. Homicz, R. Rehm, Effects of finite duct length and blade chord on noise generation by a rotating blade row, in: 7th Fluid and Plasma Dynamics Conference, 555, 1974.

[12] G. F. Homicz, J. A. Lordi, A note on the radiative directivity patterns of duct acoustic modes, J. Sound Vib. 41 (3) (1975) 283-290.

[13] S. T. Hocter, Exact and approximate directivity patterns of the sound radiated from a cylindrical duct, J. Sound Vib. 227 (2) (1999) 397-407.

[14] S. T. Hocter, Sound radiated from a cylindrical duct with Keller's geometrical theory, J. Sound Vib. 231 (5) (2000) 1243-1256.

[15] C. J. Chapman, Sound radiation from a cylindrical duct. Part 1. Ray structure of the duct modes and of the external field, J. Fluid Mech. 281 (1994) 293-311.

[16] J. B. Keller, Geometrical theory of diffraction, J. Opt. Soc. Am. 52 (2) (1962) 116-130.

[17] S. Félix, J. B. Doc, M. A. Boucher, Modeling of the multimodal radiation from an open-ended waveguide, J. Acoust. Soc. Am. 143 (6) (2018) 3520-3528.

[18] W. Duan, R. Kirby, A hybrid finite element approach to modeling sound radiation from circular and rectangular ducts, J. Acoust. Soc. Am. 131 (5) (2012) 3638.

[19] S. Sakamoto, Road traffic noise prediction model "ASJ RTN-Model 2013": Report of the Research Committee on Road Traffic Noise, Acoust. Sci. Tech. 36 (2) (2015) 49-108.

[20] Z. Maekawa, Noise reduction by screens, Appl. Acoust. 1 (3) (1968) 157-173.

[21] A. Büyükaksoy, F. Birbir, Analysis of an Impedance Loaded Parallel-Plate Waveguide Radiator, J. Electromagn. Waves Appl. 12 (11) (1998) 1509-1525.

[22] F. Birbir, A. Büyükaksoy, V. P. Chumachenko, Wiener-Hopf analysis of the two-dimensional box-like horn radiator, Int. J. Eng. Sci. 40 (1) (2002) 51-66.

[23] G. Gabard, R. J. Astley, Theoretical model for sound radiation from annular jet pipes: far-and near-field solutions, J. Fluid Mech. 549 (2006) 315-341.

[24] A. Demir, S. Rienstra, Sound Radiation from an Annular Duct with Jet Flow and a Lined Center Body, in: 12th AIAA/CEAS Aeroacoustics Conference, 2718, 2006.

[25] A. Demir, A. Büyükaksoy, Transmission of sound waves in a cylindrical duct with an acoustically lined muffler, Int. J. Eng. Sci. 41 (20) (2003) 2411-2427.

[26] A. Demir, A. Büyükaksoy, Wiener-Hopf approach for predicting the transmission loss of a circular silencer with a locally reacting lining. Int. J. Eng. Sci. 43 (5-6) (2005) 398-416.

[27] C. Yang, J. Pan, L. Cheng, A mechanism study of sound wave-trapping barriers, J. Acoust. Soc. Am. 134 (3) (2013) 1960-1969.

[28] T. A. Khan, M. Ayub, K. Jilani, E-polarized plane wave diffraction by an impedance loaded parallel-plate waveguide located in cold plasma, Phys. Scr. 89 (9) (2014) 095207.

[29] R. Mittra, S. W. Lee, Analytical techniques in the theory of guided waves, Macmillan, New York, 1971, pp. 91-113.

[30] C. Yang, Y. Fang, C. Zhao, X. Zhang, On modeling the sound propagation through a lined duct with a modified Ingard-Myers boundary condition, J. Sound Vib. 424 (2018) 173-191.

[31] X. Wang, D. Mao, W. Yu, Z. Jiang, Sound barriers from materials of inhomogeneous impedance, J. Acoust. Soc. Am. 137 (6) (2015) 3190-3197.

[32] S. Hein, T. Hohage, W. Koch, On resonances in open systems, J. Fluid Mech. 506 (2004) 255-284.

[33] A. B. Bauer, Impedance theory and measurements on porous acoustic liners. J. Aircr. 14 (8) (1977) 720-728.

[34] C. K. Tam, K. A. Kurbatskii, K. K. Ahuja, R. J. Gaeta Jr, A numerical and experimental investigation of the dissipation mechanisms of resonant acoustic liners, J. Sound Vib. 245 (3) (2001) 545-557.

[35] E. J. Brambley, Well-posed boundary condition for acoustic liners in straight ducts with flow, AIAA J. 49 (6) (2011) 1272-1282.

[36] K. Attenborough, Acoustical impedance models for outdoor ground surfaces, J. Sound Vib. 99 (4) (1985) 521-544.

[37] J. Guo, X. Zhang, Y. Fang, R. Fattah, Reflected wave manipulation by inhomogeneous impedance via varying-depth acoustic liners, J. Appl. Phys. 123 (17) (2018) 174902.

[38] X. Wang, W. Yu, X. Zhu, Z. Jiang, D. Mao, Effects of ceiling phase gradients on the acoustic environment on roadside balconies. J. Acoust. Soc. Am. 141 (2) (2017) EL146-EL152.